Characterization of Zinc Carboxylates in an Oil Paint Test Panel

Christine Romano, Thomas Lam, G. Asher Newsome, Joshua A. Taillon, Nicole Little & Jia-sun Tsang

ORIGINAL RESEARCH OR TREATMENT PAPER

Check for updates

Characterization of Zinc Carboxylates in an Oil Paint Test Panel

Christine Romano[1], Thomas Lam[1], G. Asher Newsome [1], Joshua A. Taillon [2], Nicole Little [1] and Jia-sun Tsang[1]

[1]Museum Conservation Institute, Smithsonian Institution, Suitland, MD, USA; [2]Material Measurement Laboratory, National Institute of Standards and Technology, Gaithersburg, MD, USA

ABSTRACT
Zinc (carboxylate) soaps, formed by reactions between zinc oxide (ZnO) and fatty acids in a drying oil, are known to cause deterioration in the paint layers of modern and contemporary oil paintings. This study investigates zinc carboxylates that developed in an oil painting test panel designed to mimic the aging and degradation encountered in actual works of art. Following accelerated and natural aging, protrusions were noted on the surface of the test panel. A large protrusion with erupted gel features was extracted from the test panel, mounted in top view, and then cut to reveal the sample's cross section. The gel features, which resulted from the unreacted oil binder's separation from the paint matrix, facilitated zinc carboxylate formation. Using reflectance μ-FTIR and SEM-EDX analysis, the morphologies and spatial distributions of zinc carboxylates within the gel regions of the protrusion were studied. A concentration gradient of zinc within the gel material was observed in the cross-sectional view, indicating patterns of zinc carboxylate formation and migration.

Introduction

Background

Zinc soap related deterioration poses a potential threat to nineteenth century to contemporary oil paintings containing zinc oxide (ZnO). Formed by reactions between the ZnO pigment (also known as zinc white) and fatty acids in a drying oil, zinc carboxylate soaps are known to cause brittleness, delamination, increased transparency, and protrusions in oil paintings (Shimadzu and Van Den Berg 2006; Noble and Boon 2007). In collaboration with the National Museum of African American History and Culture (NMAAHC), conservators at the Museum Conservation Institute (MCI) have undertaken technical studies that have identified zinc soap deterioration in the form of protrusions on a landscape by Robert S. Duncanson (1821–1872); transparent, deformed paint passages on several paintings by Clementine Hunter (1886–1988); and localized cracking and delamination on works by Felrath Hines (1913–1993), among other cases. The detection of zinc soaps in paintings spanning such a broad time-frame prompted conservators and conservation scientists at MCI to further investigate this phenomenon through the study of an oil paint test panel.

Zinc white came into regular use as an artists' pigment in Europe and the United States from the early to mid-nineteenth century (Kühn 1986). Technical

studies conducted at numerous institutions have identified deterioration caused by zinc soaps in modern and contemporary paintings by Pablo Picasso, Vincent van Gogh, Georgia O'Keeffe, Karel Appel, Max Beckmann, Lucio Fontana, Jackson Pollock, and many others (van der Weerd et al. 2003; Faubel et al. 2011; Muir et al. 2013; Izzo et al. 2014a, 2014b; Gabrieli et al. 2017; Salvant et al. 2017).

Zinc soap species include both amorphous zinc carboxylates, which are bonded to the oxidized, cross-linked oil network, and crystalline zinc soaps, which are highly ordered and most frequently linked to paint degradation (Hermans et al. 2015, 2016; Osmond 2019). Among the many manifestations of zinc soap-related deterioration are protruding masses that share morphological similarities with the spherical and crater-like lead soaps, which were first characterized by conservators and scientists at the Mauritshuis Royal Picture Gallery (Heeren et al. 1999; Boon et al. 2002). Localized cracking and delamination, blisters, craters, and translucent gel-like materials have also been noted in zinc soap-containing paint films (Osmond, Keune, and Boon 2005; Rogala et al. 2010; Faubel et al. 2011). In a sealed can of early twentieth century oleoresinous paint containing ZnO, Dredge et al. (2013) note 'seed-like lumps' of zinc oleate, and a brittle, waxy layer of coalesced zinc stearates. Paint manufacturers have similarly acknowledged the

development of 'seeding' or 'seediness' when commercial zinc white oil paint is exposed to water (Hess 1979). In addition to visibly altering the appearance of a painting's surface, zinc carboxylates can also be present within the paint layers without any visible indication on the surface (Gabrieli et al. 2017).

The propagation of zinc soaps can be linked to both a painting's environment and the location and abundance of free fatty acids. Hydrolysis of the paint film, accelerated in the presence of water, produces fatty acids that are available to react with zinc ions (Zn^{2+}) from the pigment to form metal soaps (Erhardt, Tumosa, and Mecklenburg 2005). A number of researchers have demonstrated that paint layers with a low pigment volume concentration or that contain aluminum stearate additives may offer additional sources of free fatty acids within a paint system (Ordonez & Twilley 1997; Tumosa 2001; Burnstock et al. 2007; Izzo et al. 2014a; Osmond 2014, 2019). As a result, zinc soaps are often detected along interfaces of paint layers that are rich in fatty acids. It has been proposed that the formation of crystalline zinc soaps (which exhibit a carboxylate peak maximum at 1540 cm^{-1} in the infrared spectrum) is contingent upon the availability of free fatty acids in the oil binder, whereas amorphous zinc soap species (identified by their broad carboxylate peak maximum around 1585 cm^{-1} in the infrared spectrum) occur when Zn^{2+} binds to the ionomeric polymer network of the linseed oil binder (Casadio, Bellot-Gurlet, and Paris 2019; Hermans et al. 2019). Zinc stearate and palmitate are among the more widely reported zinc soap species in the literature, though shorter chain and unsaturated fatty acid soaps are also known to occur (Keune and Boon 2007; Rogala et al. 2010; Hermans et al. 2018).

Many different scientific approaches have been undertaken in the study of metal soaps. Zinc soaps have been investigated with Fourier transform infrared (FTIR) and Raman spectroscopy, which have proved to be important tools for confirming and differentiating the types of zinc soaps (Robinet and Corbeil 2003; Faubel et al. 2011; Otero et al. 2014; Hermans et al. 2015; Gabrieli et al. 2017). Crystallinity and phase behaviors, linked to the maturity of zinc soaps, have been studied with X-ray diffraction (XRD) and differential scanning calorimetry (DSC), revealing different crystallization behaviors (Barman and Vasudevan 2006; Nelson and Taylor 2014; Hermans et al. 2016). The identification of fatty acids and carboxylates related to metal soaps has been undertaken with gas chromatography-mass spectrometry (GC-MS) (Maines et al. 2011; La Nasa et al. 2018). Cross-sectional analysis has also been a useful means for correlating visual information with spectroscopic analysis, and studies undertaken as early as 1999 with secondary ion mass spectrometry (SIMS) have identified and spatially mapped metal carboxylate species in correlation with other imaging and analytical techniques (Heeren

et al. 1999; van der Weerd et al. 2003; Keune 2005; Keune and Boon 2007; Noble and Boon 2007). Finally, studies of the effects of accelerated aging on model paint systems have evaluated time-based spectroscopic studies of saponification and paint, the effects of heat and water, and optimizations of instrumental methodologies (Keune et al. 2009; Osmond 2012; Casadio, Bellot-Gurlet, and Paris 2019).

Focus of investigation

This study investigates zinc carboxylates that developed under known conditions from a chosen set of materials following accelerated and ambient aging over several years. Deterioration phenomena such as delamination were not observed in the test panel and were thus not investigated. The aim of this study was to identify the distribution and migration of zinc carboxylates into a fatty acid-rich environment within a large mounted protrusion sample. Differences in phase and location of zinc carboxylate species were also studied to better understand this particular type of degradation, should it be encountered on actual works of art.

Methods and materials

Test panel

A test panel was created in 2014 with the goal of simulating a typical paint layering system in which zinc soaps could potentially form. A stretched cotton canvas was primed with a commercial lead white oil ground (Rublev Oil Colors) and set aside to dry for two years prior to the creation of the test panel. Artist grade zinc oxide pigment (Fezandie and Sperrle) was dispersed in cold-pressed linseed oil (Kremer Pigmente) using a glass muller on a glass slab until a thickness and rheology consistent with oil paint was achieved. The hand-mulled zinc white paint was applied to the panel by brush in a region measuring 4.5×5.8 cm. After nine days of curing in ambient conditions, cadmium red deep commercial oil paint (Winsor & Newton), chosen based on the observation by Rogala et al. (2010) of cadmium red's selective degradation when layered over zinc white, was painted over the hand-mulled zinc white layer. The completed test panel was allowed to cure for five days before undergoing accelerated aging.

Exposure of zinc oxide oil paint films to elevated humidity and heat is known to cause the propagation of zinc carboxylates and influence the crystallization rate of metal soaps (Osmond 2012; Baij et al. 2018; Hermans et al. 2019; Casadio, Bellot-Gurlet, and Paris 2019). Accelerated aging was undertaken to expose the panel to fluctuating humidity and temperature in order for degradation to be observed in a timely

manner (Feller 1995). The test panel was placed in an ESPEC Criterion temperature/humidity benchtop unit that cycled between 15°C and 20% relative humidity (RH) and 50°C and 80% RH for 10 h with a 2-hour ramp between set-points for a total of 672 h. After accelerated aging, no visible deterioration was detected on the surface under magnification. In 2018, after four years of natural aging in ambient indoor conditions, the test panel was examined and numerous protrusions were observed on the surface, in addition to a large, irregularly-shaped protrusion containing gel features.

Mounted protrusion with gel features

One notable sample – a large, irregularly shaped protrusion with translucent, gel-like features that erupted from the paint – was selected for study. It was removed from the test panel and embedded in Bio-Plastic® resin (Figure 1). The sample was mounted in a top (or satellite) configuration. Dry polishing of the embedded sample was carried out judiciously to reveal more of the gel-like features using a method described by Tsang, Friedberg, and Lam (2019). The polished, top-mounted sample was then cut and polished along the sample's edge to observe the cross section (Figure 1). The top and cross-sectional surfaces of the sample were analyzed with µ-FTIR non-contact mapping in reflectance mode and scanning electron microscopy with energy dispersive X-ray spectroscopy (SEM-EDX) to correlate organic and inorganic data related to the distribution of zinc carboxylates present within the gel material.

Unmounted samples

Additional samples were removed from the test panel and kept unmounted for corollary analysis and comparison. Among the samples were a gel material that formed adjacent to the mounted protrusion sample; additional small, round protrusions without gel features; and cadmium red and zinc white paint layers in visually good condition (referred to hereafter as baseline paint). Each of these three types of samples was analyzed with attenuated total reflection (ATR)-FTIR and direct analysis in real-time mass spectrometry (DART-MS). The original cold-pressed linseed oil used in the construction of the test panel and commercial zinc soaps obtained for reference were also analyzed with these instrumental techniques for comparison. For a complete list of instruments and experimental conditions, see Appendix 1: Materials and methods.

Results and discussion

The results of this study are compiled in such a way as to build a correlative dataset using several instrumental

and imaging-based techniques. The first set of data presented are photomicrographs, which serve to establish a visual aid and vocabulary for discussing the features of the mounted sample containing the gel material (Figure 1). DART-MS, a rapid method of sampling and ionization for mass spectrometry, is presented next as a confirmation of fatty acid species present in the organic component of the sample. Data from reflectance FTIR with µ-FTIR imaging is presented to illustrate spatial information from the sample's organic features, and ATR-FTIR analysis of site-specific unmounted samples is used to correlate peaks between modes. Finally, SEM-EDX contributes chemical imaging and elemental quantification, linking spatial elemental data with organic data collected from FTIR techniques.

Optical microscopy of mounted sample

In 2018, the test panel was examined with a Hirox optical microscope, and approximately 24 protrusions were visible on the lowest range objective (6.3 mm field of view). The protrusions ranged from 10 to 600 µm in diameter and between 90 and 300 µm in height, with the majority measuring about 20×90 µm. In many cases, the zinc white paint erupted through the upper cadmium red layer, and translucent features were occasionally visible on the top surfaces of the protrusions (Figure 1(A)). Preliminary analysis of the sample with ultraviolet radiation revealed a strong greenish visible fluorescence in the zinc white, typical of acicular zinc oxide particles produced by the Direct/American pigment processing method, while the translucent, gel-containing areas fluoresced weakly (Rogala 2019).

The large, irregularly-shaped protrusion exhibited three erupted areas of zinc white paint, each of which contained a translucent, gel material core. The protrusion measured approximately 800 µm in width by 300 µm in height from the surface. A fissure-like feature was noted in the smallest eruption (Figure 1 (a)). The large, gel-containing protrusion in Figure 1(a) was mounted in top-view configuration and partially dry polished to reveal portions of the underlying gel material immediately below the surface (Figure 1(b)). The blue arrows in Figure 1(a-b) indicate corresponding areas before and after the sample was extracted, embedded, and polished. The top view sample was cut along the bottom edge (according to the orientation of Figure 1(b)) and partially dry polished to expose the cross section (Figure 1(d)). From the cross section, the interior morphology of the gel material, measuring approximately 100 µm in depth, could be discerned.

DART-MS of unmounted samples

The use of mass spectrometry techniques such as gas chromatography-mass spectrometry (GC-MS) in the
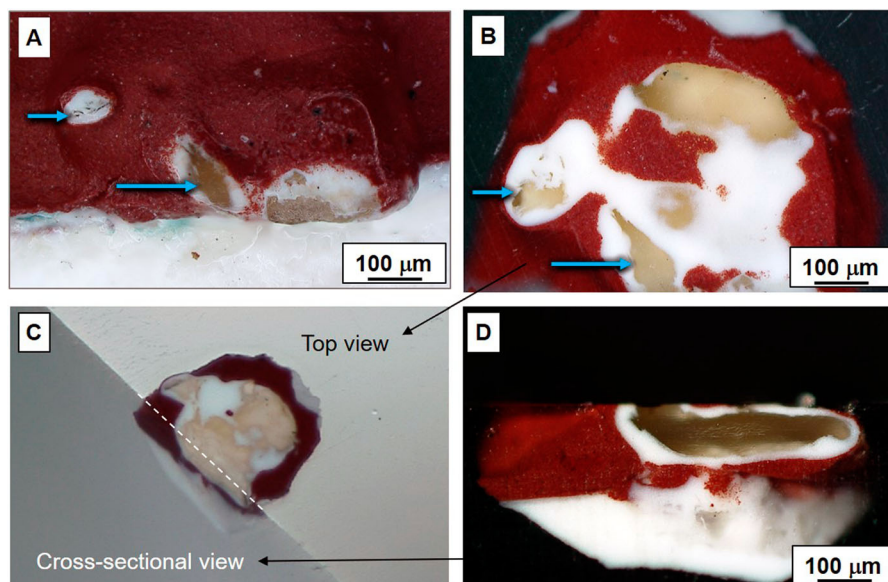
Figure 1. (A) Irregular protrusion with gel material prior to sampling. The small eruption in the upper left contained a translucent fissure-like feature (small blue arrow). A larger eruption containing a gel material is indicated by the longer blue arrow. (B) Top-view mounted sample of irregular protrusion shown in Figure 1(A) (blue arrows correspond to features in 1(A); dark areas correspond to Bio-Plastic® mounting resin). (C) Photograph of mounted sample at oblique angle after analysis illustrating the two polished planes that were studied. The sample was embedded in top-view and cut along the bottom edge (according to the orientation shown in 1 (B)) to reveal the interior of the gel material in cross section view. (D) Cross-sectional view of sample. Dark areas correspond to Bio-Plastic® mounting resin.

characterizations of paint and related degradation products is well established (Schilling, Mazurek, and Learner 2007; Bonaduce and Andreotti 2009). In this study, DART-MS was used to compare fatty acid species observed in commercial zinc soaps with those found in the oil paint test panel. This is a method for ambient mass spectrometry in which materials are rapidly sampled at atmospheric pressure with little to no preparation (Cody, Laramée, and Dupont Durst 2005). DART produces intact ions for simultaneous high-resolution MS detection, instead of chromatographically separating species for highly fragmentary electron ionization with GC-MS, allowing rapid sampling and detection of analytes, typically within 1–2 min (Maric et al. 2018). The technique, which does not discriminate between free and metal-coordinated forms, required no procedural derivatization of the samples.

Unmounted samples (approximately 5 µg) of the gel material, protrusion, and baseline paint were collected on the tip of a thin, metal probe and analyzed with DART-MS for comparison with the mounted sample. Cold-pressed linseed oil used in the creation of the test panel and samples of commercial zinc stearate were analyzed for reference and comparison. Among the numerous variations in possible isomers, all samples were found to contain C12-C27 fatty acid species. The most abundant species detected in the test panel samples were C16 and C18 fatty acids, consistent with paint based on linseed oil. The gel material most likely contained zinc stearate and/or palmitate species. The samples' organic constituents detected

by DART-MS were paired with reflectance µ-FTIR mapping and SEM-EDX, allowing for visualization of distributed materials within the mounted gel-containing sample.

ATR-FTIR of unmounted samples

Initial analysis by ATR-FTIR of loose, unmounted samples of a gel material, a small protrusion, and baseline paint from the test panel revealed network-coordinated amorphous zinc carboxylates (broad, asymmetric carboxylate stretching (v_a COO) around 1585 cm^{-1}) to be present in all samples, with evidence of partial crystallinity in the gel material (sharp v_a COO absorption at 1539 cm^{-1}) (Supplemental Figures 3–5). Other absorptions associated with zinc carboxylates, including CH_2 bending (δ) around 1455 cm^{-1} and symmetric carboxylate stretching (v_s COO) at 1400 cm^{-1}, were also noted in each of the unmounted samples (Robinet and Corbeil 2003; Hermans et al. 2016).

Reflectance µ-FTIR of mounted sample

To determine the distribution of zinc carboxylate species within the gel material of the mounted sample, analysis by reflectance µ-FTIR was undertaken. Many paint cross section studies utilizing reflectance µ-FTIR have been carried out in recent decades (Heeren et al. 1999; van der Weerd et al. 2002; 2004; Keune and Boon 2004, 2007; Rosi et al. 2011). It should be noted that relative to ATR-FTIR data, reflectance mode µ-FTIR spectra frequently contain artifacts, such

as interference, scattering, and high levels of noise, and both absorption and/or reflectance bands may be present (Heeren et al. 1999). Therefore, to successfully utilize reflectance μ-FTIR in this study, all reflectance spectra collected from the test panel cross sections were compared to ATR spectra of corresponding loose, unmounted samples. This process enabled the matching of peak absorptions between the two modes and demonstrated the circumstances under which artifacts occurred. Due to limitations in data interpretation by the instrument's proprietary software, which only processed non-normalized, single channel output data, multivariate analysis of the collected data was undertaken.

Prior to investigating the embedded sample, commercial zinc stearate was analyzed in both reflectance and ATR modes, and the spectra were compared (Figure 2). In Figure 2, corresponding peaks between reflectance and ATR spectra for the commercial zinc stearate are noted with blue dotted lines and shading. Both spectra exhibited three strong absorptions in the same region, though the reflectance spectrum is notably noisier and relative intensity scaling between the peaks is not preserved. These differences are not unexpected, however, as reflectance FTIR is a non-contact technique, whereas ATR generates data through contact. The reflectance spectrum exhibited several v_a COO peaks between 1510 and 1600 cm^{-1} compared to the single peak noted in this region in ATR mode (Figure 2, shaded blue). This is consistent with other observations made over the course of this study in which the strongest peak in ATR was present in reflectance mode as a broader absorption. However, most other spectral features were preserved,
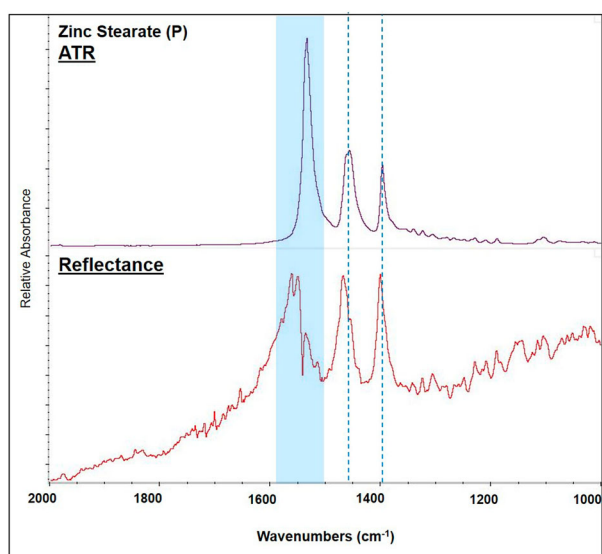
most notably δ CH$_2$ absorptions around 1455 cm^{-1} and v_s COO absorptions around 1400 cm^{-1}.

Following the analysis of the commercial zinc stearate reference sample, the top and cross-sectional views of the mounted sample were analyzed using reflectance FTIR with μ-FTIR mapping. Spectra were collected in a raster-scan map and correlated with visible material phases and their boundaries. The identification of saponified regions in the map allowed for the visualization of zinc carboxylate development and migration within the gel material. The raw spectral data were then analyzed using a multi-dimensional data algorithm that generated component maps and component spectra representative of algorithmically-defined material phases present in the top and cross section views of the sample (Figure 3).

Multivariate analysis of μ-FTIR data

The precision mechanical mapping stage on the FTIR instrument enables the automation of spectral data collection from wide areas of a sample into a multidimensional data structure known as a hyperspectral data cube. Besides visualization, the advantage of such spectral mapping arises from the statistical power gained by collecting many independent measurements from the sample, typically hundreds or thousands of spectra. Many statistical analysis methods have been developed to better extract information from such hyperspectral data (Gendrin, Roggo, and Collet 2008). Indeed, such methods typically form the basis of the 'phase mapping' technologies offered by some vendors within their proprietary software (Taillon 2018). Multivariate techniques analyze all the spectral information of the data cube at once, rather than point by point, finding statistical correlations between the spectra and separating the data into a linear combination of factors (plus noise). Each factor has a spectral signature as well as a spatial distribution, which can be visualized as material phase-specific maps. These factors are estimates of the 'true' or 'pure' spectral components and their spatial distribution, which typically cannot be measured directly due to their proximity to the other phases, limited spatial resolution, and overlap of spectral features throughout the map. In this work, a non-negative matrix factorization (NMF) algorithm (Lee and Seung 1999) was used to separate the hyperspectral reflectance FTIR data with HyperSpy, an open-source Python (programming language) library widely used for multi-dimensional data analysis (de la Pena et al. 2018) (See Supplemental Data Figs.1–2 for full HyperSpy code). This method was applied to both the top and cross-sectional reflectance μ-FTIR data cubes. The analysis effectively removed noise and allowed distinct

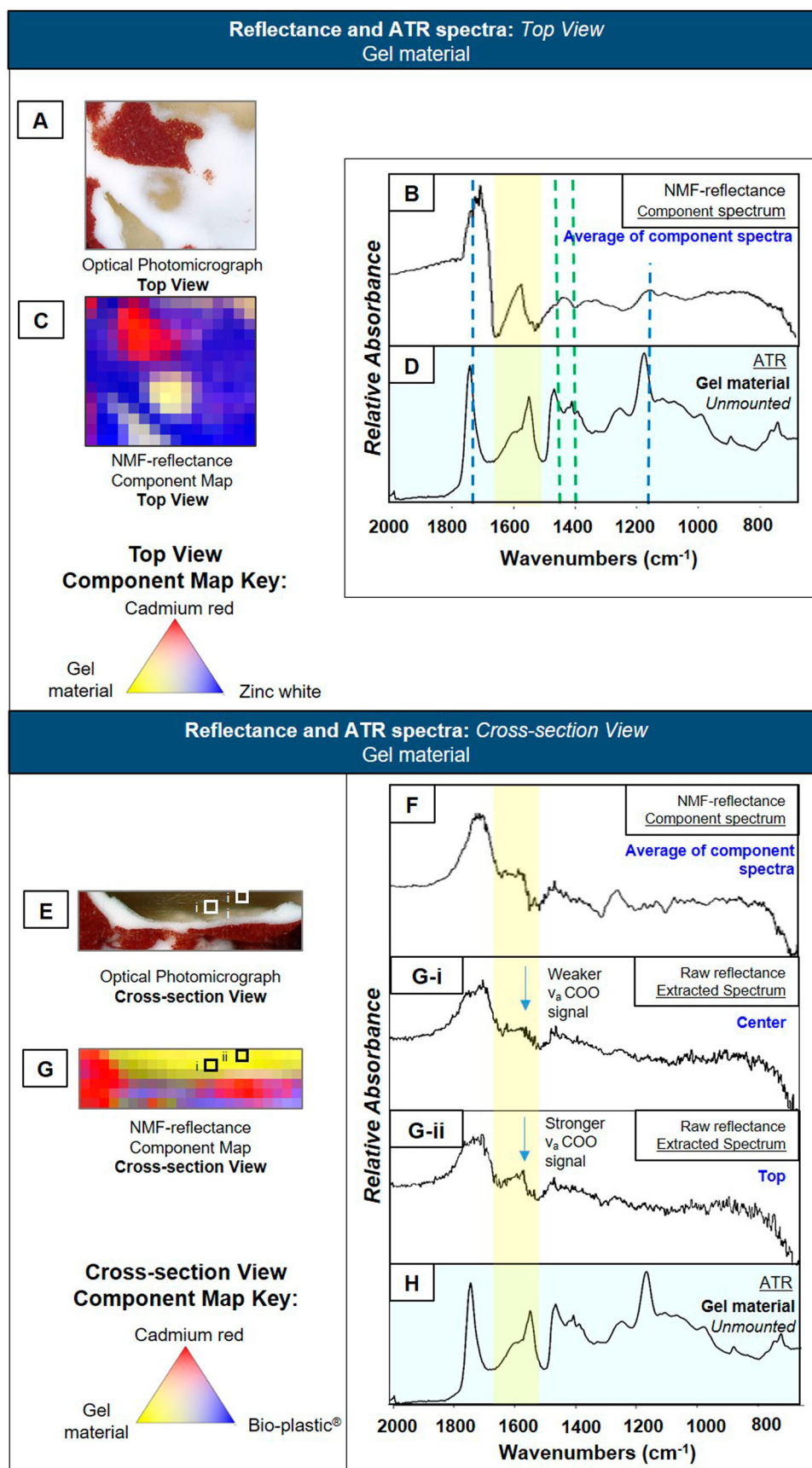**Figure 2.** Comparison of commercial zinc stearate reference sample in ATR mode and Reflectance μ-FTIR modes. Blue shading and dotted lines indicate corresponding peaks between modes, though with some shifting and scaling differences.

Figure 3. Comparison of NMF-reflectance component spectra and maps for the gel material with ATR spectra and optical photomicrographs. (A) Optical image of top view. (B) Component spectrum of the gel material phase, as determined by NMF analysis of the data cube. (C) Mixed component map for the top view from NMF data cube separation. The horizontal field width (HFW) of the collected data is 300 μm, containing 240 unique spectral measurements. (D) ATR-FTIR spectrum of an extracted sample from the gel material. (E) Optical image of cross-sectional view. (F) Component spectrum from the gel material phase, as determined by NMF analysis. (G) Mixed component map of cross-sectional view from NMF data cube separation. The horizontal field width (HFW) of the collected data is 440 μm, containing 138 measurements. (G-i): Raw extracted reflectance μ-FTIR spectrum from the boxed area 'i' at the center of the gel material phase. (G-ii): Raw extracted reflectance μ-FTIR spectrum from the boxed area 'ii' at the upper edge of the gel material phase. H. ATR-FTIR spectrum of an extracted sample from the gel material.

spectral features and mathematically representative spatial distribution maps to be presented.

For this study, the primary purpose of analyzing the collected μ-FTIR data was to generate visual and spectral data on the zinc soap-containing gel material phase and its boundaries. Rather than mapping for a functional group, the NMF algorithm detects the pattern or spectral signature for a given material in the sample, such as the gel material. A representative map of the gel material's spatial distribution within the analyzed area is then generated (referred to as an NMF-reflectance component map), which corresponds to a mathematically averaged spectrum created from all spectral signatures for that particular material phase (referred to as an NMF-reflectance component spectrum).

The hyperspectral reflectance μ-FTIR component spectra and raw spectra are presented from the gel material phase in Figure 3. The maps, though pixelated in appearance due to the mapping step size and the μ-FTIR aperture diameter (40×40 μm), generally correspond well with the visible material phases in the optical photomicrographs (Figure 3(a, c, and e, g)). The mixed NMF-reflectance component map for the top view (Figure 3(c)) is color-weighted based on the relative intensity of the three algorithmically-defined material phases: cadmium red region (represented in red), zinc white region (blue), and the gel material region (yellow). The mixed NMF-reflectance component map for the cross section view (Figure 3(g)) is similarly color-weighted based on the relative intensity of three material phases: cadmium red region (represented in red), Bio-plastic® region (blue), and the gel material region (yellow). Unlike the top view, the cross-sectional view contained Bio-Plastic® resin. In this case, because the gel material and zinc white paint both could contain a linseed oil and zinc carboxylate signal, the algorithm more readily identified the Bio-plastic® resin as the third component and mapped it as a distinct phase due to its mathematical difference from the other materials (see also Supplemental Figure 2). Linseed oil features, including the characteristic triglyceride ester bonds indicated by the blue dotted line (c. 1160 cm^{-1}) in Figure 3(b and d), are present in both the ATR spectrum of the gel material and in the averaged component spectrum of the top view, which notably includes zinc white paint. This feature is not found in Figure 3(f) due to the inclusion of Bio-Plastic® in the spectral averaging.

It should also be noted the dimensions of the zinc white paint layer in cross section are at or below 40 μm, which may have been difficult for the NMF algorithm to resolve given the μ-FTIR aperture size.

The NMF-reflectance component spectrum of the gel phase in top view is compared with an ATR spectrum of a sample of unmounted gel material in Figure 3(b and d). Zinc carboxylates are clearly apparent in the top view sample. The ATR spectrum (Figure 3(d)) shows both broad and sharp absorptions at 1585 and 1539 cm^{-1} respectively, indicating both amorphous and crystalline zinc carboxylates, while the NMF-reflectance spectrum (Figure 3(b)) shows a strong, broad metal carboxylate peak at 1561 cm^{-1}, highlighted with a yellow band. The reflectance spectrum in Figure 3(b) also shows a broad absorption between 1400 and 1450 cm^{-1} (indicated by green dotted lines) that may correspond to the δ CH$_2$ around 1455 cm^{-1} and/or the ν$_s$ COO absorptions around 1400 cm^{-1} in the ATR spectrum of the gel.

Zinc carboxylate concentration gradient in mounted sample

In the cross-sectional view, single-point raw reflectance spectra (Figure 3(g-i) and Figure 3(g-ii)) have been extracted from the boxed regions of the mixed component map in Figure 3(g). Though the spectrum is unprocessed and significant noise is present, a broad peak can be discerned in the ν$_a$ COO region at approximately 1580 cm^{-1} in both spectra. The peak is more clearly defined in Figure 3(g-ii), which was extracted from the upper edge of the gel material, located in close proximity to the zinc white paint layer. In contrast, Figure 3(g-i), taken from the center of the gel, exhibits a weaker and less distinct ν$_a$ COO region, consistent with its greater distance from a Zn^{2+} ion source in the zinc white paint. The NMF-reflectance component spectrum (Figure 3(f)) for the gel material in cross section is noisier than the component spectrum for the top view (Figure 3(b)). Because the gel material in top view shared an interface with the zinc white layer, it was able to react along the entire interfacing surface due to the immediate proximity and availability of Zn^{2+} ions in the zinc white layer. Conversely, the interior core of the gel material did not have immediately adjacent Zn^{2+} ions with which it could react. Therefore, the noisier signal in Figure 3(f) is derived from the averaging of the zinc carboxylate-rich outer edges of the gel with the linseed oil signal from the interior of the gel.

ATR-FTIR analysis of unmounted gel material

Many absorptions associated with the oil binder were present in the ATR spectra. Relative to the CH$_2$ vibrations around 2920 cm^{-1} (not shown), the ATR spectrum for the gel sample in Figure 3(d) shows higher intensities for ester linkages than would be expected for an aged material (Meilunas, Bentsen, and Steinberg 1990; Learner 2004). Generally, a reduction in intensity and broadening of absorptions at 1160 and 1240 cm^{-1}, and the development of a shoulder at 1715 cm^{-1} on the ester carbonyl are characteristic of aged oil paint films due to triglyceride hydrolysis and the formation of degradation products

(Meilunas, Bentsen, and Steinberg 1990; Mazzeo et al. 2008). This expected trend of the oil binder's reduced peak intensity is clearly visible in spectra for the baseline paint; however, the gel material exhibits peak intensities more typical of unaged linseed oil (see Supplemental Data Figures 3–5). Relative to the alkyl bands in the ATR spectrum of the gel material, the C–O absorption at 1160 cm^{-1} is stronger and sharper than expected, the absorption at 1240 cm^{-1} is more pronounced than in cured films, and the ester carbonyl stretch at 1732 cm^{-1} is strong, sharp, and lacks a shoulder, suggesting the sample has not undergone hydrolysis and oxidation to the same extent as the surrounding materials, perhaps due to its location within the zinc white paint layer, which prevented any contact with the air. The 1160 cm^{-1} peak is also visible, though broadened and attenuated, in the NMF-reflectance spectrum of the top view (Figure 3 (b)). A similar mixture of zinc carboxylates and unreacted esters was also observed in the IR spectrum of a model Zn-ethyl linoleate complex in the work of MacDonald et al. (2016).

SEM-EDX of mounted sample

SEM-EDX with elemental mapping was carried out to complement optical and organic analytical data, including the observed zinc carboxylate gradient. The mounted sample containing the gel material was analyzed on both its top and cross-sectional surfaces using optical microscopy and SEM techniques, as presented in Figure 4. The backscatter electron (BSE) micrograph of both the top (Figure 4(c)) and cross-sectional view (Figure 4(d)) reveal the varying contrasts of the features present. SEM-EDX provided elemental information on the materials present. In Figure 4(c and d), areas of red paint exhibiting the brightest contrast contained cadmium (Cd), selenium (Se), barium (Ba), calcium (Ca), magnesium (Mg), and sulfur (S), consistent with a commercial cadmium red paint, while the white paint regions exhibiting mid-level contrast contained primarily Zn, typical of a handmade zinc white paint free of additives. The gel material exhibited the darkest contrast (Figure 4 (c, d)) and contained carbon (C), oxygen (O), Zn, S, and chlorine (Cl). The detection of Zn in the gel material by SEM-EDX complements findings from FTIR analysis, where distributions of zinc carboxylates were identified in the gel material.

The composite EDX maps, presented in false color for C (blue), O (white), Zn (green), and Cd (red), are shown in top view (Figure 4(e)) and in cross section (4f). These maps confirm the gel features are present as irregularly-shaped pools containing a C-rich material inside the zinc white layer, a portion of which includes zinc carboxylates. A table of the mass fraction

concentrations in the gel, Bio-Plastic®, and zinc white is located in the supplemental data (Supplemental Table 1.)

The presence of Cl in the gel material was detected in mass fractions of approximately 1%, as seen in the EDX intensity maps in Figures 4(g and h). Low concentrations of sulfur (S) were also detected in the gel material (Supplemental Table 1). Previous studies have also detected Cl inside lead and zinc soap aggregates (Osmond, Keune, and Boon 2005; Keune and Boon 2007; Helwig et al. 2014). Keune and Boon (2007) suggest lead chloride mineral phases may be present in lead soap protrusions, possibly from contaminants in the pigment. In this study, Cl was not detected in any of the original paint materials (zinc white, cadmium red, or the lead white ground). It is proposed, then, that the observed concentration of Cl may originate from the painting's interaction with the environment, which in turn suggests the zinc soaps may have an affinity for chlorine.

Zn concentration gradient in mounted sample

An EDX profile scan was carried out on the cross-sectional view beginning at the top of gel and terminating just above the zinc white layer (Figure 5). A series of 10×10 μm manually selected regions (Figure 5(b), boxed areas 1–5) were collected in incremental positions along the height of the gel with extracted background normalized EDX spectra of the corresponding positions. Corresponding Zn signal counts for each boxed region were overlaid for comparison in Figure 5(a). Much like the carboxylate gradient observed in the μ-FTIR maps, a Zn concentration gradient was observed in the cross-sectional view of the gel material, but not in the top view (Figure 5(d)). The mass fraction of Zn was approximately 6.5% at the top of the gel feature, then decreased to 3.5% Zn toward the core, increasing again to 7.6% Zn at the bottom (Figure 5 (c)). This trend was also noted in six additional profile scans (Supplemental Figure 6), supporting these observations of a Zn concentration gradient.

Phase separation and zinc carboxylate migration

In order for the C-rich gel material to form in the mounted sample, the linseed oil medium would have had to first separate from the bulk paint. In the case of the test panel, it is possible the lack of dispersants in the handmade zinc white paint contributed to the separation of the oil. Phase separation by synersis has also been proposed by Williams (1988), where oil paint components become incompatible through shrinkage, oxidation, or changes in polarity, causing them to separate phases and migrate. The separation
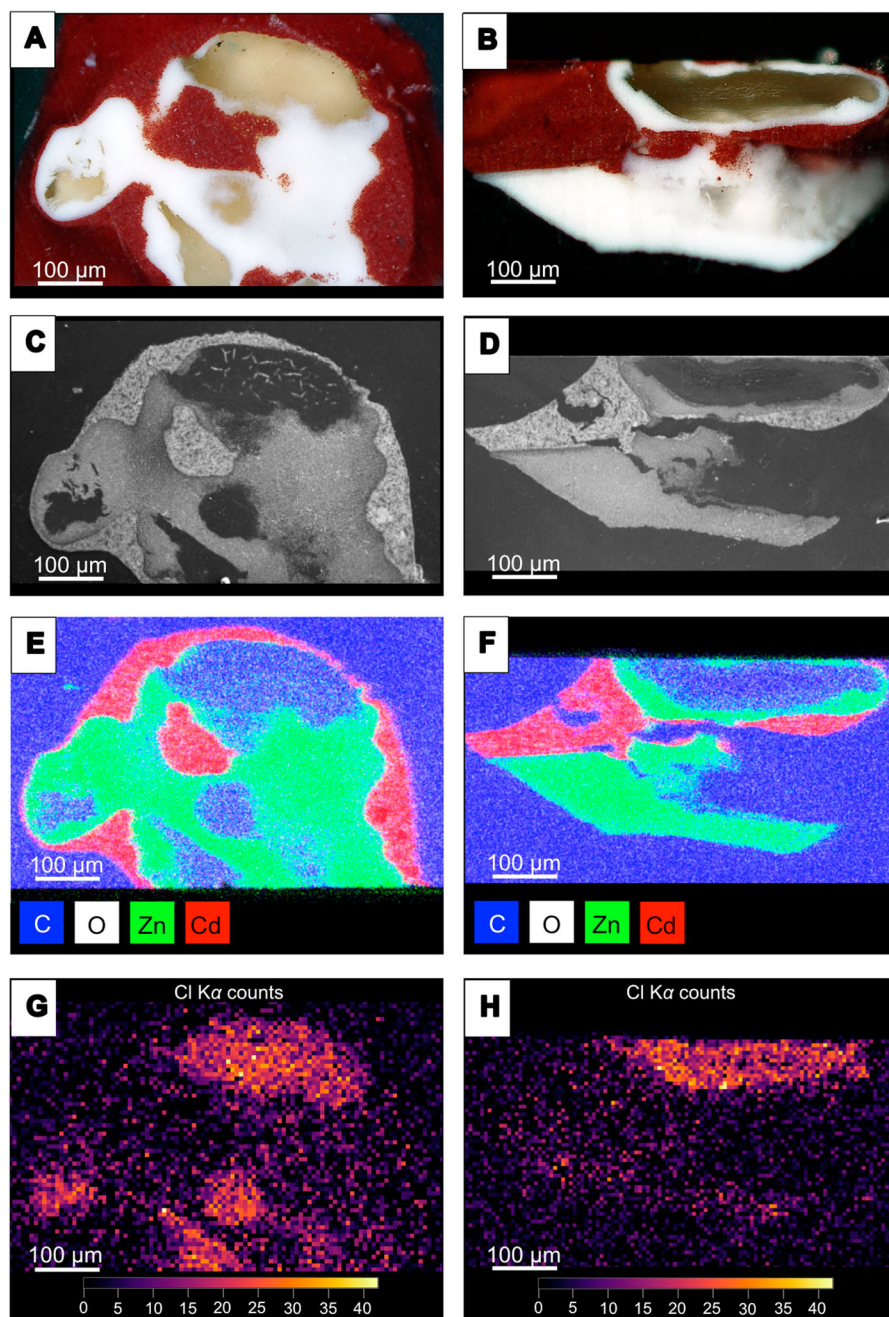
Figure 4. Optical photomicrographs and chemical maps of the top and cross section views presented at the same scale. (A) Optical micrograph of top view of the sample. (B) Optical micrograph of the cross-sectional view of the sample. (C) BSE micrograph of top view of the sample. (D) BSE micrograph of the cross-sectional view of the sample. (E) Composite EDX maps for the top view. (F) Composite EDX maps for the cross-sectional view. (G) Intensity map showing higher chlorine concentrations within the gel regions of the top view. (H) Intensity map showing higher concentrations of chlorine within the gel regions of the cross-sectional view, processed as in Figure 4(g).

of the oil media from the paint may have initiated saponification by its availability as a solvent. Following phase separation, the ZnO particles from the zinc white layer would have been able to dissolve into the C-rich region and saponify, reacting to form products of zinc carboxylates from the available fatty acids. With the saponification of Zn and the phase-separated linseed oil, a significant volume increase would occur, forcing the paint film upward (van der Weerd et al. 2003). The proclivity of zinc soaps to migrate in fatty acid-rich environments was also observed in the work

of Mills et al. (2008), where Zn was detected in a gel material from a phase-separated model paint film to which zinc stearate had been added. Research by Hermans et al. (2019), whose findings are based on a similar scenario of low concentrations of ZnO in a linseed oil-rich environment, suggests that Zn^{2+} and fatty acids from the paint film are encouraged to migrate toward growing aggregates as soon as zinc soap precipitation begins.

In this study, it is proposed from FTIR and SEM-EDX analysis of the cross section that the center of the gel
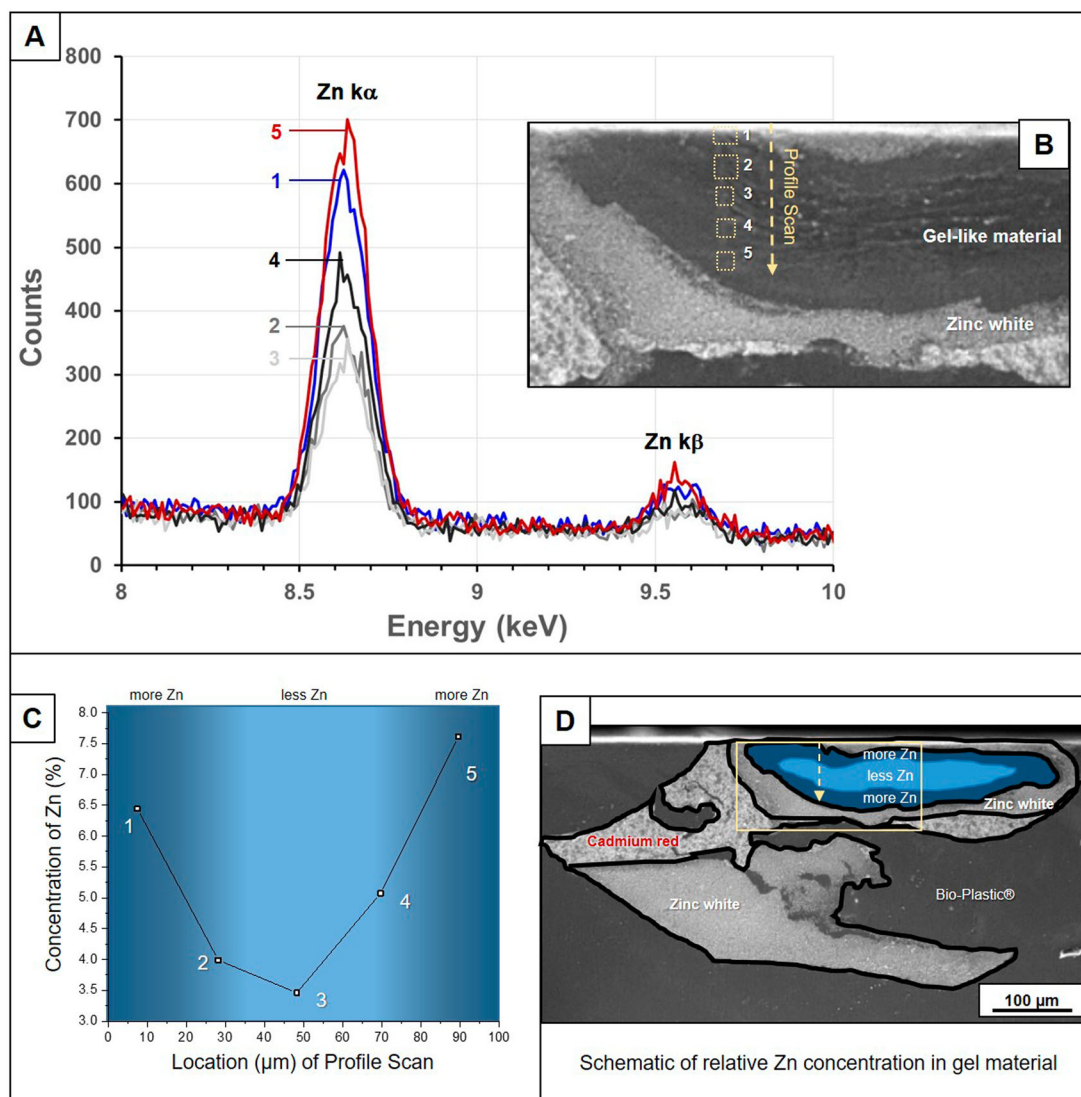
Figure 5. (A) Overlay of increasing and decreasing Zn signal collected during EDX profile scan of areas 1 through 5 in the gel material. (B) BSE image of cross-sectional view with overlaid EDX profile scan (dark contrast regions represent the gel material, medium contrast is zinc white, and brightest contrast is cadmium red). The area shown represents the boxed region of the schematic in Figure 5(D). (C) Semi-quantified EDX mass fraction for Zn corresponding to areas 1 through 5 in the profile scan. Note the lowest concentration of Zn is present at the center of gel (boxed region 3). (D) Schematic of higher and lower areas of Zn concentration within the gel material overlaid on a BSE image of the cross-sectional view.

material has not reacted to form zinc carboxylates to the same extent as the outer edges of the gel. A mass fraction of only 3.5% Zn was detected at the center of the gel material. This concentration is considerably less than the 10% mass fraction expected from the stoichiometric percentage of Zn in zinc stearate, $Zn(C_{18}H_{35}O_2)_2$, for example, leaving a substantial remaining mass to be the linseed oil binder. These remaining fatty acid reactants in the gel material have the potential to continue forming zinc soaps, which could possibly result in further degradation and deformation of the paint layer. The zinc carboxylate concentration gradient provides some indication of the manner in which zinc carboxylates form and migrate, and suggests the saponification is in a relatively early stage, despite some apparent degree of crystallinity.

Conclusion

This study characterized the phase-separated, unreacted linseed oil within a gel material that reacted to form amorphous and crystalline zinc carboxylates on an oil paint test panel following accelerated aging and several subsequent years of continued aging in ambient conditions.

ATR-FTIR indicated both amorphous and crystalline zinc carboxylates were present within the gel material. The approach of mounting the test panel sample in top view and slicing it to reveal the cross section proved crucial for a spatially locating zinc carboxylates within the gel material. The ability to collect correlative data from two planes of the sample with μ-FTIR mapping, SEM-EDX imaging, and optical microscopy resulted in a better understanding of zinc carboxylate diffusion in a fatty acid-rich environment.

Multivariate analysis of μ-FTIR data from the mounted sample detected a zinc carboxylate gradient in the cross-sectional view of the gel material, where the edges were rich in zinc carboxylates, and the center contained quantities of unreacted linseed oil. A corollary Zn concentration gradient was detected by SEM-EDX, with more Zn present in the edges of the gel than in the center. In contrast, the top view of the sample showed a uniform distribution of Zn, due to its previous direct contact with the ZnO paint. These findings suggest media separation precedes zinc carboxylate formation, given the distribution of zinc carboxylates around the perimeter of the gel material. Elemental mapping also revealed the affinity of environmental Cl for zinc carboxylate-containing regions of the gel material.

The observation of zinc soaps diffusing into the fatty acid-rich interior of the gel material begs the question of whether the Zn ions will ultimately form a homogenous crystalline mass of zinc soaps at the core. Further work is needed to better understand this possibility as well as other types of deterioration associated with zinc soaps, including cracking, delamination, and increased translucency of the paint layer.

Acknowledgments

Disclosure statement

No potential conflict of interest was reported by the authors.

ORCID

G. Asher Newsome http://orcid.org/0000-0003-1683-2197
Joshua A. Taillon http://orcid.org/0000-0002-5185-4503
Nicole Little http://orcid.org/0000-0002-9533-3187

Data availability statement

The data that support the findings of this study are openly available in the NIST Public Data Repository at https://doi.org/10.18434/M32082

References

Baij, Lambert, Joen J. Hermans, Katrien Keune, and Piet Iedema. 2018. "Time-Dependent ATR-FTIR Spectroscopic Studies on Fatty Acid Diffusion and the Formation of Metal Soaps in Oil Paint Model Systems." *Angewandte Chemie International Edition* 57: 7351–7354.

Barman, S., and S. Vasudevan. 2006. "Contrasting Melting Behavior of Zinc Stearate and Zinc Oleate." *The Journal of Physical Chemistry B* 110 (2): 651–654.

Bonaduce, Ilaria, and Alessia Andreotti. 2009. "Py-GC/MS of Organic Paint Binders." Chap. 11 in *Organic Mass Spectrometry in Art and Archaeology*, edited by Maria Perla Colombini and Francesca Modungo, 304–326. New York: Wiley.

Boon, Jaap J., Jaap van der Weerd, Katrien Keune, Petria Noble, and Jørgen Wadum. 2002. "Mechanical and Chemical Changes in Old Master Paintings: Dissolution, Metal Soap Formation and Remineralization Processes in Lead Pigmented Ground/Intermediate Paint Layers of 17th Century Paintings." In *13th Triennial Meeting of the ICOM Committee for Conservation in Rio De Janeiro Preprints*, edited by R. Vontobel, 401–406. London: James & James.

Burnstock, Aviva, Klaas Jan van den Berg, Suzan de Groot, and Louise Wijnberg. 2007. "An Investigation of Water Sensitive Oil Paints in 20th Century Paintings." In *Modern Paints Uncovered: Proceedings from the Modern Paints Uncovered Symposium, Tate Modern, London, May 16–19, 2006*, edited by Thomas J. S. Learner, Patricia Smithen, Jay W. Krueger, and Michael R. Schilling, 177–188. Los Angeles: Getty Publications.

Casadio, Francesca, Ludovic Bellot-Gurlet, and Céline Paris. 2019. "Factors Affecting the Reactivity of Zinc Oxide with Different Drying Oils: A Vibrational Spectroscopy Study." In *Metal Soaps in Art: Conservation and Research*, edited by Francesca Casadio, Katrien Keune, Petria Noble, Annelies van Loon, Ella Hendriks, Silvia Centeno, and Gillian Osmond, 153–170. Switzerland: Springer.

Cody, Robert B., James A. Laramée, and H. Dupont Durst. 2005. "Versatile New Ion Source for the Analysis of Materials in Open air Under Ambient Conditions." *Analytical Chemistry* 77 (8): 2297–2302.

de la Pena, Francisco, Vidar Tonaas Fauske, Pierre Burdet, Eric Prestat, Petras Jokubauskas, Magnus Nord, Tomas Ostasevicius, et al. 2018. "HyperSpy v1.4.1." *Open-source Software for Multi-Dimensional Data Analysis*, doi:10.5281/zenodo.1469364.

Dredge, Paula, Michael R. Schilling, Gwénaëlle Gautier, Joy Mazurek, Tom Learner, and Richard Wuhrer. 2013. "Lifting the Lids Off Ripolin: A Collection of Paint From Sidney Nolan's Studio." *Journal of the American Institute for Conservation* 52 (4): 213–226.

Erhardt, David, Charles S. Tumosa, and Marion F. Mecklenburg. 2005. "Long-term Chemical and Physical Processes in oil Paint Films." *Studies in Conservation* 50 (2): 143–150.

Faubel, Werner, Rolf Simon, Stefan Heissler, Frank Friedrich, Peter G. Weidler, Hans Becker, and Wolfhardt Schmidt. 2011. "Protrusions in a Painting by Max Beckmann Examined with Confocal μ-XRF." *Journal of Analytical Atomic Spectrometry* 26 (5): 942–948.

Feller, Robert L. 1995. *Accelerated Aging: Photochemical and Thermal Aspects*. Los Angeles, CA: Getty.

Gabrieli, Francesca, Francesca Rosi, Alessandra Vichi, Laura Cartechini, Luciano Pensabene Buemi, Sergei G. Kazarian, and Costanza Miliani. 2017. "Revealing the Nature and Distribution of Metal Carboxylates in Jackson Pollock's Alchemy (1947) by Micro-Attenuated Total Reflection FT-IR Spectroscopic Imaging." *Analytical Chemistry* 89 (2): 1283–1289.

Gendrin, Christelle, Yves Roggo, and Christophe Collet. 2008. "Pharmaceutical Applications of Vibrational Chemical Imaging and Chemometrics: A Review." *Journal of*

Pharmaceutical and Biomedical Analysis 48 (3): 533–553. doi:10.1016/j.jpba.2008.08.014.

Heeren, R., J. J. Boon, P. Noble, and J. Wadum. 1999. "Integrating Imaging FTIR and Secondary Ion Mass Spectrometry for the Analysis of Embedded Paint Cross-Sections." In *ICOM Committee for Conservation, 12th Triennial Meeting, Preprints*, edited by J. Bridgland and J. Brown, 228–233. London: James & James.

Helwig, Kate, Jennifer Poulin, Marie-Claude Corbeil, Elizabeth Moffatt, and Dominique Duguay. 2014. "Conservation Issues in Several Twentieth-Century Canadian Oil Paintings: The Role of Zinc Carboxylate Reaction Products." In *Issues in Contemporary Oil Paint*, edited by Aviva Burnstock, Matthijs de Keijzer, Jay Krueger, Tom Learner, Alberto de Tagle, Gunnar Heydenreich, and Klaas Jan van den Berg, 167–184. Switzerland: Springer.

Hermans, Joen J., Katrien Keune, Annelies van Loon, and Piet D. Iedema. 2015. "An Infrared Spectroscopic Study of the Nature of Zinc Carboxylates in Oil Paintings." *Journal of Analytical Atomic Spectrometry* 30 (7): 1600–1608.

Hermans, Joen J., Katrien Keune, Annelies van Loon, and Piet D. Iedema. 2016. "The Crystallization of Metal Soaps and Fatty Acids in Oil Paint Model Systems." *Physical Chemistry Chemical Physics* 18 (16): 10896–10905.

Hermans, Joen J., Katrien Keune, Annelies van Loon, and Piet D. Iedema. 2019. "Towards a Complete Molecular Model for the Formation of Metal Soaps in Oil Paints." In *Metal Soaps in Art: Conservation and Research*, edited by Francesca Casadio, Katrien Keune, Petria Noble, Annelies van Loon, Ella Hendriks, Silvia Centeno, and Gillian Osmond, 47–67. Switzerland: Springer.

Hermans, Joen J., Gillian Osmond, Annelies van Loon, Piet Iedema, Robyn Chapman, John Drennan, Kevin Jack, et al. 2018. "Electron Microscopy Imaging of Zinc Soaps Nucleation in oil Paint." *Microscopy and Microanalysis* 24 (3): 318–322.

Hess, Manfred. 1979. "Seediness, Bittiness, Pigment Flocculation." In *Hess's Paint Film Defects, Their Causes and Cure*, 16–18. New York: Halsted Press.

Izzo, Francesca Caterina, Barbara Ferriani, Klaas Jan Van den Berg, Henk Van Keulen, and Elisabetta Zendri. 2014a. "20th Century Artists' Oil Paints: the Case of the Olii by Lucio Fontana." *Journal of Cultural Heritage* 15 (5): 557–563.

Izzo, Francesca Caterina, Klaas Jan van den Berg, Henk van Keulen, Barbara Ferriani, and Elisabetta Zendri. 2014b. "Modern Oil Paints–Formulations, Organic Additives and Degradation: Some Case Studies." In *Issues in Contemporary Oil Paint*, edited by Aviva Burnstock, Matthijs de Keijzer, Jay Krueger, Tom Learner, Alberto de Tagle, Gunnar Heydenreich, and Klaas Jan van den Berg, 167–184. Switzerland: Springer.

Keune, Katrien. 2005. "Metal Soap Aggregates in Oil Paintings from the 15th 20th Century." Chapter 5 in *Binding Medium, Pigments and Metal Soaps Characterised and Localised in Paint Cross-sections*. PhD diss., University of Amsterdam.

Keune, Katrien, and Jaap J. Boon. 2004. "Imaging Secondary ion Mass Spectrometry of a Paint Cross Section Taken From an Early Netherlandish Painting by Rogier van der Weyden." *Analytical Chemistry* 76 (5): 1374–1385.

Keune, Katrien, and Jaap J. Boon. 2007. "Analytical Imaging Studies of Cross-Sections of Paintings Affected by Lead Soap Aggregate Formation." *Studies in Conservation* 52 (3): 161–176.

Keune, Katrien, Frank Hoogland, Jaap J Boon, D. Peggie, and Catherine Higgitt. 2009. "Evaluation of the 'Added Value' of SIMS: A Mass Spectrometric and Spectroscopic Study of an Unusual Naples Yellow oil Paint Reconstruction." *International Journal of Mass Spectrometry* 284 (1–3): 22–34.

Kühn, Hermann. 1986. "Zinc White." In *Artists' Pigments. A Handbook of Their History and Characteristics*, edited by Robert L. Feller. Washington, DC: National Gallery of Art. 169–186.

La Nasa, Jacopo, Francesca Modugno, Matteo Aloisi, Anna Lluveras-Tenorio, and Ilaria Bonaduce. 2018. "Development of a GC/MS Method for the Qualitative and Quantitative Analysis of Mixtures of Free Fatty Acids and Metal Soaps in Paint Samples." *Analytica Chimica Acta* 1001: 51–58.

Learner, Thomas J. 2004. *Analysis of Modern Paints*. Los Angeles, CA: Getty.

Lee, Daniel D., and H. Sebastian Seung. 1999. "Learning the Parts of Objects by Non-Negative Matrix Factorization." *Nature* 401 (6755): 788–791.

MacDonald, Margaret G., Michael R. Palmer, Matthew R. Suchomel, and Barbara H. Berrie. 2016. "Reaction of Pb(II) and Zn(II) with Ethyl Linoleate To Form Structured Hybrid Inorganic–Organic Complexes: A Model for Degradation in Historic Paint Films." *ACS Omega* 1 (3): 344–350.

Maines, Christopher A., Dawn Rogala, Susan Lake, and Marion Mecklenburg. 2011. "Deterioration in Abstract Expressionist Paintings: Analysis of Zinc Oxide Paint Layers in Works from the Collection of the Hirshhorn Museum and Sculpture Garden, Smithsonian Institution." *MRS Online Proceedings Library Archive* (1319): 275–284.

Maric, Mark, James Marano, Robert B. Cody, and Candice Bridge. 2018. "DART-MS: A New Analytical Technique for Forensic Paint Analysis." *Analytical Chemistry* 90 (11): 6877–6884.

Mazzeo, Rocco, S. Prati, M. Quaranta, E. Joseph, E. Kendix, and M. Galeotti. 2008. "Attenuated Total Reflection Micro FTIR Characterisation of Pigment–Binder Interaction in Reconstructed Paint Films." *Analytical and Bioanalytical Chemistry* 392 (1–2): 65–76.

Meilunas, Raymond J., James G. Bentsen, and Arthur Steinberg. 1990. "Analysis of Aged Paint Binders by FTIR Spectroscopy." *Studies in Conservation* 35 (1): 33–51.

Mills, Laura, Aviva Burnstock, Suzan de Groot, Luc Megens, Madeleine Bisschoff, Henk van Keulen, Felipe Duarte, and Klaas Jan van den Berg. 2008. "Water Sensitivity of Modern Artists' Oil Paints." *ICOM Committee for Conservation* 2: 651–659.

Muir, Kimberley, Allison Langley, Anikó Bezur, Francesca Casadio, John Delaney, and Gwénaëlle Gautier. 2013. "Scientifically Investigating Picasso's Suspected use of Ripolin House Paints in Still Life, 1922 and The Red Armchair, 1931." *Journal of the American Institute for Conservation* 52 (3): 156–172.

Nelson, Peter N., and Richard A. Taylor. 2014. "Theories and Experimental Investigations of the Structural and Thermotropic Mesomorphic Phase Behaviors of Metal Carboxylates." *Applied Petrochemical Research* 4 (3): 253–285.

Noble, Petria, and Jaap J. Boon. 2007. "Metal Soap Degradation of Oil Paintings: Aggregates, Increased Transparency and Efflorescence." In *Paintings Specialty Group Postprints from the 35th AIC Annual Meeting*, Richmond, VA, USA.

Ordonez, Eugena, and John Twilley. 1997. "Clarifying the Haze. Efflorescence on Works of art." *Analytical Chemistry* 69 (13): 416A–422A.

Osmond, Gillian. 2012. "Zinc White: A Review of Zinc Oxide Pigment Properties and Implications for Stability in Oil-Based Paintings." *AICCM Bulletin* 33 (1): 20–29.

Osmond, Gillian. 2019. "Zinc Soaps: An Overview of Zinc Oxide Reactivity and Consequences of Soap Formation in Oil-Based Paintings." In *Metal Soaps in Art: Conservation and Research*, edited by Francesca Casadio, Katrien Keune, Petria Noble, Annelies van Loon, Ella Hendriks, Silvia Centeno, and Gillian Osmond, 25–46. Switzerland: Springer.

Osmond, Gillian, Jaap J. Boon, Ljiljana Puskar, and John Drennan. 2012. "Metal Stearate Distributions in Modern Artists' Oil Paints: Surface and Cross-Sectional Investigation of Reference Paint Films Using Conventional and Synchrotron Infrared Microspectroscopy." *Applied Spectroscopy* 66 (10): 1136–1144.

Osmond, Gillian. 2014. "Zinc White and the Influence of Paint Composition for Stability in Oil Based Media." In *Issues in Contemporary Oil Paint*, edited by Aviva Burnstock, Matthijs de Keijzer, Jay Krueger, Tom Learner, Alberto de Tagle, Gunnar Heydenreich, and Klaas Jan van den Berg, 263–281. Switzerland: Springer.

Osmond, Gillian, Katrien Keune, and Jaap J Boon. 2005. "A Study of Zinc Soap Aggregates in a Late 19th Century Painting by R.G. Rivers at the Queensland Art Gallery." *AICCM Bulletin* 29 (1): 37–46.

Otero, Vanessa, Diogo Sanches, Cristina Montagner, Márcia Vilarigues, Leslie Carlyle, João A. Lopes, and Maria J. Melo. 2014. "Characterisation of Metal Carboxylates by Raman and Infrared Spectroscopy in Works of art." *Journal of Raman Spectroscopy* 45 (11–12): 1197–1206.

Robinet, Laurianne, and Marie-Claude Corbeil. 2003. "The Characterization of Metal Soaps." *Studies in Conservation* 48 (1): 23–40.

Rogala, Dawn V., 2019. "Everything Old is New Again: Revisiting a Historical Symposium on Zinc Oxide Oil Paint Films." In *Metal Soaps in Art: Conservation and Research*, edited by Francesca Casadio, Katrien Keune, Petria Noble, Annelies van Loon, Ella Hendriks, Silvia Centeno, and Gillian Osmond, 315–328. Switzerland: Springer.

Rogala, Dawn, Susan Lake, Christopher Maines, and Marion Mecklenburg. 2010. "Condition Problems Related to Zinc Oxide Underlayers: Examination of Selected Abstract Expressionist Paintings From the Collection of the Hirshhorn Museum and Sculpture Garden, Smithsonian Institution." *Journal of the American Institute for Conservation* 49 (2): 96–113.

Rosi, Francesca, Arianna Federici, Brunetto G. Brunetti, Antonio Sgamellotti, Sergio Clementi, and Costanza Miliani. 2011. "Multivariate Chemical Mapping of Pigments and Binders in Easel Painting Cross-Sections by Micro IR Reflection Spectroscopy." *Analytical and Bioanalytical Chemistry* 399 (9): 3133–3145.

Salvant, Johanna, Marc Walton, Dale Kronkright, Chia-Kai Yeh, Fengqiang Li, Oliver Cossairt, and Aggelos K. Katsaggelos. 2017. "Photometric Stereo by UV-Induced Fluorescence to Detect Protrusions on Georgia O'Keeffe's Paintings." *arXiv preprint arXiv:*1711.08103.

Schilling, Michael R., Joy Mazurek, and Thomas J. Learner. 2007. "Studies of Modern Oil-Based Artists' Paint Media by Gas Chromatography/Mass Spectrometry." In *Modern Paints Uncovered: Proceedings from the Modern Paints Uncovered Symposium*, edited by Thomas J. S. Learner, Patricia Smithen, Jay W. Krueger, and Michael R. Schilling, 129–139. Los Angeles: Getty Publications.

Schindelin, Johannes, Ignacio Arganda-Carreras, Erwin Frise, Verena Kaynig, Mark Longair, Tobias Pietzsch, Stephan Preibisch, et al. 2012. "Fiji: An Open-Source Platform for Biological-Image Analysis." *Nature Methods* 9 (7): 676–682.

Shimadzu, Y., and K. J. Van Den Berg. 2006. "On Metal Soap Related Colour and Transparency Changes in a 19th C Painting by Millais." *Reporting Highlights of the De Mayerne Programme* 2006: 43–52.

Taillon, Joshua A. 2018. "An Open Evaluation of Hyperspectral Unmixing Strategies for EDS Analysis." *Microscopy and Microanalysis* 24 (S1): 752–753.

Tsang, Jia-sun, Elle Friedberg, and Thomas Lam. 2019. "An Easy-to-Use Method for Preparing Paint Cross Sections." *Journal of the American Institute for Conservation* 58 (8): 123–131. doi:10.1080/01971360.2018.1564198.

Tumosa, Charles S. 2001. "A Brief History of Aluminum Stearates as a Component of Paint." *WAAC Newsletter* 23 (3): 10–11.

van der Weerd, Jaap, H. Brammer, Jaap J. Boon, and Ron M.A. Heeren. 2002. "Fourier Transform Infrared Microscopic Imaging of an Embedded Paint Cross-Section." *Applied Spectroscopy* 56 (3): 275–283.

van der Weerd, Jaap, Muriel Geldof, L. Struik van der Loeff, Ron MA Heeren, and Jaap J. Boon. 2003. "Zinc Soap Aggregate Formation in Falling Leaves (les Alyscamps) by Vincent van Gogh." *Zeitschrift für Kunsttechnologie und Konservierung: ZKK* 17 (2): 407–416.

van der Weerd, Jaap, Ron M.A. Heeren, and Jaap J. Boon. 2004. "Preparation Methods and Accessories for the Infrared Spectroscopic Analysis of Multi-Layer Paint Films." *Studies in Conservation* 49 (3): 193–210.

Williams, Scott R. 1988. "Bloom, Blushes, Transferred Images and Mouldy Surfaces." *Proceedings of the 14th Annual IIC-CG Conference*, edited by J. G. Wellheiser, Toronto Area Conservation Group of the International Institute for Conservation of Historic and Artistic Works - Canadian Group, 65–84. Toronto, Ontario: IIC-CG.

Appendix I. Materials and methods

Materials

Powdered zinc soap samples from Sigma Aldrich (PO Box 14508, St. Louis, MO 63178, USA) (zinc stearate (zinc octadecanoate) 'purum' (Lot #SZBE3290 V), zinc stearate 'technical grade' (Lot #MKBH0073 V), and zinc palmitate (zinc hexadecanoate) (Lot #CDS003313)) served as references for this study. These reference zinc soaps were analyzed with various instrumental techniques and compared with test samples. Additionally, original materials used in the construction of the test panel, including cold-pressed linseed oil from Kremer Pigmente (247 W 29th St C, New York, NY 10001, USA), Zinc oxide (Fezandie and Sperrle) obtained from the Forbes Pigment Collection at SUNY Buffalo State College, and Winsor & Newton brand Cadmium red oil paint were also used for reference. Cross sections were mounted in Bio-Plastic® liquid casting resin and catalyst by Ward's Science (5100 W Henrietta Rd, West Henrietta, NY 14586, USA).

Methods

Microscopy was performed with a HIROX KH-8700 Digital Microscope with the MXG-2500REZ dual illumination lens and 2.11 Mega-pixel CCD sensor. The microscope is equipped with a motorized z control, which allows for the collection of a

focal stack that can be rendered into a 3D image with the HIROX software.

μ-Fourier transform infrared (FTIR) non-contact mapping in reflectance mode was carried out with a Thermo Nicolet 6700 FTIR spectrometer equipped with a mercury cadmium telluride type A (MCT-A) detector, in addition to attenuated total reflection (ATR)-FTIR. The mapping analysis of the embedded samples was carried out in a reflection mode with 500 scans taken from 4000 to 650 cm^{-1}, at a spectral resolution of 1.928 cm^{-1}. Mapping on uncorrected data was performed using a 40×40 μm aperture with an overlapping step size of 20 μm in the x and y axes. The FTIR maps were analyzed using HyperSpy, an open source Python-based software package for hyperspectral data processing (www.hyperspy. org). The component maps were imported into Fiji (open source software – https://fiji.sc/) to form a tri-color (red, blue, yellow) component map (Schindelin et al. 2012). Site-specific samples were also extracted for attenuated total reflection (ATR-FTIR) and transmission through an infrared microscope (μ-FTIR) using the Thermo Nicolet 6700 FTIR spectrometer with Golden Gate ATR and MTC-A detector. The data was collected at 4 cm^{-1} spectral resolution, using 64 scans in ATR-FTIR mode.

Scanning electron microscopy with energy dispersive X-ray spectroscopy (SEM-EDX) was performed on carbon-coated embedded samples in high vacuum mode using a Hitachi S3700-N SEM. EDX was performed using a Bruker XFlash 6 | 60 detector with Esprit software. Samples were analyzed at a 15 kV primary electron accelerating voltage. Normalized semi-quantitative analyses were calculated by the technique of P/B-ZAF (peak to background atomic number, absorption, and fluorescence correction) model performed on selected regions. Integrated X-ray counts at the Cl-Kα line were plotted after spatial binning by a factor of 8 in both the x and y dimensions. The background signal was subtracted, and the counts within the Cl-Kα peak were integrated to obtain a value at each pixel representing the total number of Cl-Kα x-rays detected at that position.

Direct analysis in real time (DART) MS was performed with a DART 100 ion source operated by an SVP controller (IonSense, Saugus, MA) mounted in transmission mode in front of a high-resolution LTQ Orbitrap Velos mass spectrometer (Thermo Fisher Scientific, Waltham, MA) fitted with a differentially-pumped Vapur interface. The ceramic insulator cap of the DART was set back 7 mm from the ceramic transfer tube of the interface. The helium ionization gas was set to a heater temperature of 300 ℃. Extracted site-specific solid sample masses on the order of 5 μg were pierced with a tungsten wire, mounted, and translated axially into the DART gas stream for analysis. MS data was acquired at 30000 resolving power with a maximum ion trap fill time of 100 ms.